Measurement of HgXe excimer potentials

L. K. Lam[a] and Alan Gallagher[b]

Joint Institute for Laboratory Astrophysics, University of Colorado and National Bureau of Standards, Boulder, Colorado 80309

R. Drullinger

Time and Frequency Division, National Bureau of Standards, Boulder, Colorado 80302
(Received 19 January 1978)

The HgXe excimer band at 270 nm has been studied in fluorescence following optical excitation of the Hg $^3P_1$ level. From the temperature dependence of the normalized fluorescence band shape, the potential curves of the $^3O^+$ excimer state and the $^1O^+$ ground state are inferred. A binding energy of 1400 ± 100 cm^{-1} is found for the $^3O^+$ state.

I. INTRODUCTION

The profile of the 253.7 nm line of Hg broadened by Xe has been extensively studied; references can be found in Ref. 1. More recently, interest in the HgXe excimer as an efficient uv pump source or high power laser has generated a series of studies in the far wing profile at Xe densities of 1 atm and more.[2–4] However, most of these studies were mainly concerned with kinetics in the presence of a high energy deposition. From these data the excimer binding was poorly determined and the excimer potential was unknown, nor are calculated excited state potentials to be found in the literature. The data reported here can be used to calculate excited-state densities, gain coefficients, and vibrational temperatures from measured emission intensities in high-power systems. Some characteristics of the potentials can also be determined, in particular the $^3O^+$ state binding and the relationship between the $^3O^+$ and $^1O^+$ potentials at each R. The R dependence of these potentials is estimated from the data, but due to the unknown variation of the $^3O^+ - {}^1O^+$ transition moment with internuclear separation, this R dependence is not well established from these experiments.

We have measured the temperature dependence of the 270 nm band fluorescence intensity (as a continuum) normalized to the optically thin 253.7 nm atomic line intensity. We excite Hg 6^3P_1 atoms optically; these then undergo three-body association with two Xe atoms to form bound HgXe excimer molecules. At the Xe densities of these experiments these bound excimers are dissociated by Xe collisions more rapidly than their spontaneous emission rate. The density of the excimer thus comes to equilibrium with the Hg 6^3P_1 density, allowing straightforward interpretations of the band intensity in terms of the classical Franck–Condon principle and classical statistical mechanics. This optical excitation method produces a simple excimer band spectrum and clearly identifies the excimer state as associated with the 6^3P_1 atomic state. Similar methods have been used to determine the potentials of other metal excimer systems.[5,6]

II. HgXe*

Although no calculations are available for the HgXe excimer molecules, a schematic indicating the expected type of behavior is drawn in Fig. 1. In the large R region, where $\Delta\Omega$ splittings are smaller than the $^3P_{2,1,0}$ splittings, Hund's case (c) coupling applies,[7] and for simplicity this has been used to label the states at all R. In the large R region the states arising from the 6^3P_0 and 6^3P_2 are nonradiative, but 6^3P_1 radiates at $\sim 10^{-7}$ sec^{-1} due to a small admixture of the $^1P_1$ configuration. At smaller R the $^3O^-$ state arising from $^3P_0$ would still be nonradiative in case (c) due to symmetry, as well as the weak spin selection rules, but partial recoupling to case (a) will occur, allowing a weak transition moment. Similar statements apply to the states arising from the $^3P_2$ state. The excimer states that can be formed from the 6^3P_1 and radiate to the ground $^1O^+$ state are the $^3O^+$ and ^{31} states. These states are sometimes referred to in literature as the $^3\Pi$ and $^3\Sigma^+$ states, respectively, in Hund's case (a) coupling notations. A pure $^3\Sigma^+$ state can be expected to be predominantly repulsive, in analogy with the $^2\Sigma$ excimer states in alkali–noble gas excimers.[5] For HgXe the Hund's case (c) coupling notation is more appropriate, so that the ^{31} state has both Π and Σ components and can be expected to be somewhat attractive. The $^3O^+$ state has predominantly Π character and is expected to be much more attractive than ^{31}, in analogy to the $A^2\Pi$ states of the alkali–noble gas excimers. The 270 nm band is thus attributed to the $^3O^+ - {}^1O^+$ transition. Due to the (recoupling) sharing of transition moment between 6^3P_1 and 6^3P_2 parentage states, the $^3O^+ - {}^1O^+$ transition moment is expected to decrease with decreasing R, as has been reported for Hg$_2$ excimer radiation.[6] We expect the ^{31} state to be weakly bound; and thus to contribute very little radiation in the region of the 270 nm band. This is discussed further below.

III. THEORY OF EXCIMER BAND INTENSITY

The theory follows that in Refs. 5, 6, and 8, and is based on the classical Franck–Condon principle (or quasistatic theory of line broadening) combined with classical statistical mechanics. The fluorescent intensity at the quasistatic wing, when normalized to the atomic line intensity and Xe density, is given by
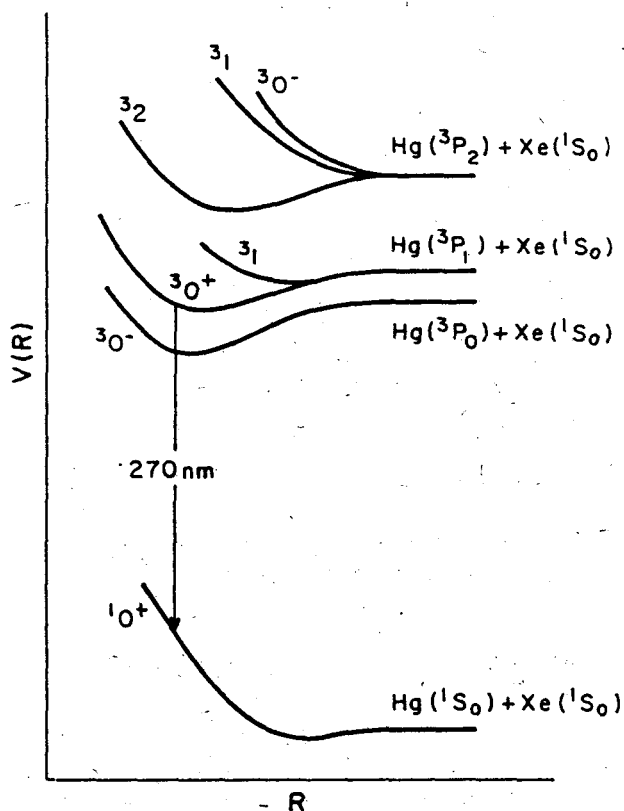
FIG. 1. A schematic diagram of the HgXe states associated with the 6 ^1S and 6 ^3P states.

$$I_N(k) = \frac{I(k)}{[Xe] \int_{line} I(k')dk'}$$

$$= \sum_i \frac{g_i}{g_A}\left(\frac{k}{k_0}\right)^4 \frac{D(k)_i}{D(k_0)} 4\pi R^2 \frac{dR}{dk} \exp[-\beta\Delta V^*(k)_i] . \quad (1)$$

Here $k = \lambda^{-1}$, $\beta = 1/k_B T$, where k_B is the Boltzmann constant, T is the gas temperature, $[Xe]$ is the xenon density, g_i and g_A are the statistical factors of the molecular state i and atomic parentage state, respectively, $D(k)_i$ is the transition dipole moment from state i at internuclear separation $R(k)$, $D(k_0)$ is the transition moment from the atomic parentage state of energy hck_0, the $^3P_1$ excitation energy, and the exponential factor is the Boltzmann population factor in the excimer state. In the present case $i = 1, 2$ refers to the $^3O^*$ and ^{31} states of $^3P_1$ atomic parentage. The relation $R(k)$ or $k(R)$ is given by the classical Franck–Condon principle as $hck = V^*(R)_i - V(R)$, where $V^*(R)_i$ and $V(R)$ are the adiabatic potentials of the excited and ground states, respectively. Also, $\Delta V^*(k)_i = V^*[R(k)]_i - hck_0$. Equation (1) applies to fluorescence from optically thin vapor and the integral is only over the atomic line. It can be easily confirmed that the actual $I_N(k)$ is equal to the apparent $I_N(k)$ observed with finite spectrometer resolution, for k in the far wing where $I(k)$ varies slowly within the instrumental resolution.

The Boltzmann factor in Eq. (1) refers to an equilibrium distribution of bound excimer states.[8] We expect this to hold in this experiment with $[Xe] \sim 10^{19}$ cm^{-3},

a radiative rate Γ_n of about 10^7 sec^{-1}, and an excimer binding D_e of $6kT$ or less. As a comparison, the NaXe* excimer at a temperature of ~ 400 °K, where $\sim 4k_B T$ equals the binding, has a collisional dissociation rate coefficient of $k_d = 3 \times 10^{-11}$ cm^{3}sec^{-1}. Such rate coefficients are expected[9] to vary as $k_d \propto \exp(-D_e/kT)$. In this experiment, at all but the lowest temperature the binding is less than $5.4kT$, so in analogy with NaXe*, $k_d \gtrsim 7 \times 10^{-12}$ cm^{3}sec^{-1}. The ratio of collisional dissociation to radiation at $[Xe] = 10^{19}$ cm^{-3} is thus $k_d[Xe]/\Gamma_M \gtrsim 7$ for a molecular radiative rate Γ_M equal to the atomic rate of 10^7 sec^{-1}. Thus, equilibrium between bound and free states should be fairly well established. At the lowest temperature for which we have taken data (~ 20 °C) this ratio is only ~ 2 and equilibration may be marginal. Uncertainties due to this will be discussed in Sec. V.

If the observed band is due to only the $^3O^* - {}^1O^*$ transition, then, from Eq. (1), $\Delta V^*(k)$ can be determined from the temperature dependence of $I_N(k)$. Since the ground-state potential variation $\Delta V(k) = \Delta V^*(k) + k - k_0$, this also establishes $\Delta V(k)$. To obtain $V^*(R)$, $I_N(k)$ can be extrapolated to $T = \infty$ and Eq. (1) integrated to give R as a function of k:

$$R^3(k) - R_1^3(k_1) = \frac{3}{4\pi}\frac{g_A}{g_M}\int_{k_1}^k \left(\frac{k_0}{k}\right)^4 \frac{D(k_0)}{D(k)} I_N(k)_{T-\infty}dk . \quad (2)$$

Here the subscript 1 refers to a reference point k_1, generally taken at the long-wavelength edge of the band where $V(R_1)$ is highly repulsive. Since $V(k_1)$ is known from the temperature dependence, it can be compared to $V(R)$ from Hg–Xe atomic beam scattering data[9] to establish $R_1(k_1)$. The unknown quantity in the integrand is the transition moment ratio $D(k_0)/D(k)$. As noted in the Introduction, the transition moment for the $^3O^*$ state is expected to be less than that of the $^3P_1$ state due to recoupling between the various excimer states that connect to the $^3P_{2,1,0}$ states. In the excimer Hg$_2^*$ the measured[6] transition moment decreases by factors of up to 3–4 as R decreases, presumably in large part for the same reason. An estimate for this $D(k)$ variation will be used below to estimate the R dependence of the potentials.

IV. EXPERIMENTAL

A low pressure 4 W germicidal lamp, with $\sim 90\%$ of its emission in the 253.7 nm line, was used as an excitation source. The spectral profile of the line was measured and found to be only moderately self-reversed with a width of ~ 1.2 cm^{-1}. This matches the Xe broadened absorption width (~ 0.4 cm^{-1}) in the mercury cell fairly well and efficient excitation can be expected. No filter was used between lamp and cell, as the instrumentally scattered lamp continuum was negligible. About 20 mW of the 253.7 nm light was collimated into the mercury cell by the collecting optics.

The mercury cell was ~ 5 cm long and 2.5 cm diameter, made of uv grade quartz, and had a sidearm of ~ 13 cm long. Mercury was triply distilled into the prebaked cell blanks, research grade Xe was introduced at a pressure measured by a bakeable capacitance manom-
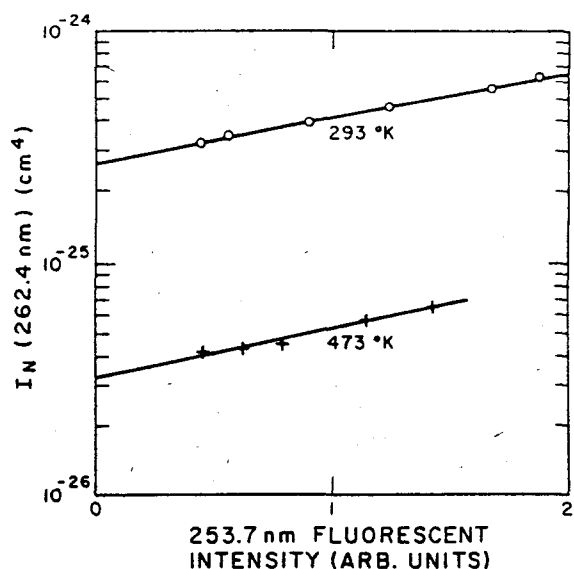
FIG. 2. Variation of molecular to atomic fluorescence intensity ratio with increasing radiation trapping for cell temperature of 293 and 473 °K.

eter, and the cell was sealed. Cells were filled with Xe densities of from 10^{17} to 10^{19} cm^{-3}.

The mercury cell was housed in an oven with the sidearm protruding into a cooled enclosure to control the cell Hg density. Collimated exciting light was imaged into the cell and fluorescence light at 90° to the incident beam was focused onto a spectrometer. Instrumentally (nonfluorescent) scattered 253.7 nm light was reduced with imaging and apertures until it was determined to be less than 1% of fluorescence. (For this determination the scattered fraction of the 313.1 nm line was measured and assumed to apply to the 253.7 nm line.)

A 2 m spectrometer typically set to 0.8 nm resolution was used to scan the spectrum. (A larger instrumental width was used to increase the weaker far wing signals at high temperatures.) The far wings of the spectrometer instrument function were measured using 253.7 nm fluorescence from a cell containing only Hg. In the far wings of the 253.7 nm line, where data are reported, the spectrometer leakage was $\sim 3 \times 10^{-5}$ of the 253.7 nm signal. This leakage of the 253.7 nm fluorescence was reduced by about a factor of 7 by inserting a Hg–Xe absorption cell between the oven and the spectrometer while taking far-wing data. The residual leakage is about 3×10^{-27} cm^4 in the units of Fig. 3. It has been subtracted from the detected signal, but the residual uncertainty is estimated as 10^{-27} cm^4 and is the primary limitation to measurements of low wing intensities. Another source of uncertainty came from leakage of other, more intense portions of the band. To accurately evaluate and subtract this would have required iterative convolution procedures and it was not attempted. However, it can be shown to be less than a 10% correction, and much less for all but the far red edge of the band.

The relative detection efficiency of the output optics, spectrometer, and photomultiplier was measured as a unit by replacing the Hg cell with a BaSO$_4$ scattering surface illuminated by a calibrated deuterium uv lamp; the spectra presented in the figures have been corrected for this detection efficiency variation.

To obtain the properly normalized spectrum, radiation trapping of the atomic line must be either negligible or accounted for. The mercury pressure could have been reduced to produce the desired optically thin conditions by cooling the sidearm reservoir. However, the migration time for the mercury out of even a heated cell and through the transition zone to the temperature defining point of the reservoir was exceedingly slow (many days). Furthermore, since the band fluorescence increases with mercury density, it would have been necessary to measure very weak signals. Consequently, the shape of the excimer band for each gas temperature was measured with the sidearm at room temperature and considerable radiation trapping. To correctly normalize the band the intensity at a single point in the band (262.4 nm) was then measured relative to the total integrated 253.7 nm intensity [the denominator in Eq. (1)] in the limit of optically thin conditions. This was done in the following way:

The fluorescence intensity from the optically thin 262.4 nm region of the band was compared to the partially trapped 253.7 nm intensity as the mercury density was varied. Data of this type for two temperatures (20 and 200 °C) are plotted in Fig. 2. In this figure $I_N(262.4$ nm$)$ is plotted as a function of 253.7 nm intensity (which is a nonlinear but monotonic index of the mercury density). This plot format has the advantage of yielding straight lines on semilog paper, thereby allowing accurate extrapolation to the optically thin, low density limit (left intercept). Complete data sets of this type were taken only for the two temperatures 20 and 200 °C, since the shape in Fig. 2 was independent of temperature. At other temperatures the $I_N(262.4$ nm$)$ intensity ratio was measured at only one or two relatively low intensities, or Hg densities, and extrapolated using the slope observed in Fig. 2.

The resulting band intensity, corrected to optically thin conditions, is given in Fig. 3. The 252–255 nm portion represents the spectrometer instrument function. The blue wing decreased more rapidly than the instrument function, so that the blue-wing intensity in Fig. 3 is only an upper limit to the actual emission spectrum. The instrumental resolution does not affect the results in the 255–285 nm region, but in the $\lambda > 285$ nm region spectrometer leakage of the 260–280 nm band is significant at the lower temperatures.

Although the mercury cell was filled at $[Xe] = 10^{19}$ cm^{-3} at room temperature, the Xe density in the cell body became lower when the cell body and sidearm were subjected to different temperatures. This reduced $[Xe]$ was calculated, from the temperatures and volume ratio of the two parts of the cell, and used in calculating $I_N(k)$ according to the definition in Eq. (1).
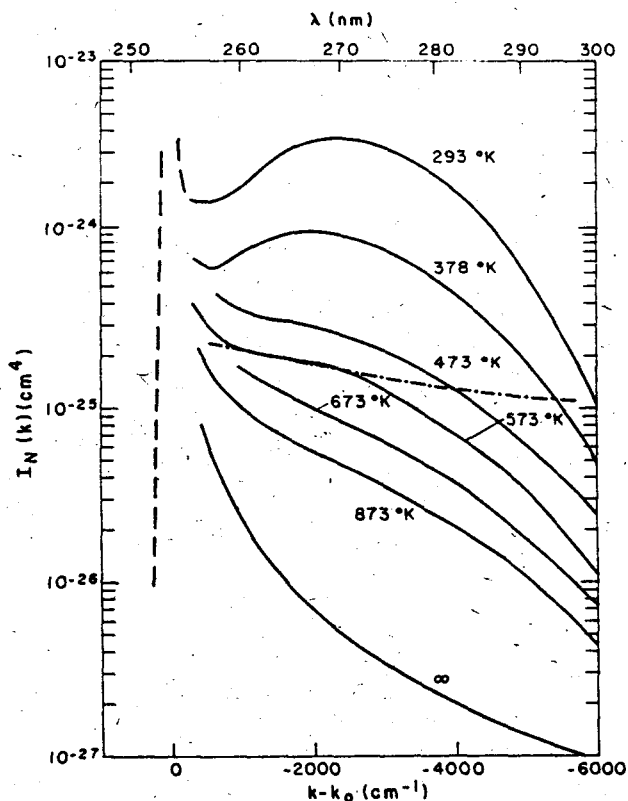
FIG. 3. Normalized emission spectrum of $6\,^3P_1$ Hg atoms in the presence of $\sim 10^{19}$ cm^{-3} of Xe. The integral $\int I(k')dk'$ is over a ± 20 Å region that encompasses the atomic line core. The dashed line represents a gain coefficient $G_\nu = 10^{-38}$ cm^5 [Hg($6\,^3P_1$)][Xe].

The reported $I_N(k)$ is related to a stimulated emission coefficient per Hg($6\,^3P_1$) density [Hg($6\,^3P_1$)] by[8]

$$\frac{G_\nu}{[\mathrm{Hg}(6\,^3P_1)]} = \left(\frac{\lambda^3}{8\pi\lambda_0}\right)\frac{I_N(k)\,\Gamma_0}{c}, \quad (3)$$

where $\Gamma_0 \cong 10^7$ sec^{-1} is the $6\,^3P_1$ state radiative rate. A line of $G_\nu/[\mathrm{Hg}(6\,^3P_1)][\mathrm{Xe}] = 10^{-38}$ cm^5 is indicated in Fig. 4 to facilitate conversion of the data to units of the stimulated emission coefficient (for a thermalized population of excimers). For example, the ratio of the band intensity $[I_N(k, T)]$ to the dashed line is $G_\nu/[\mathrm{Hg}(6\,^3P_1)][\mathrm{Xe}]$ in units of 10^{-38} cm^5.

V. DATA ANALYSIS

Excitation transfer from $6\,^3P_1$ to $6\,^3P_2$ is negligible as a result of the 0.57 eV endothermicity, but transfer to $6\,^3P_0$ is exothermic. The rate coefficient for $6\,^3P_1 \rightarrow 6\,^3P_0$ transfer due to Xe collisions has been measured[10] as less than 5×10^{-15} cm^3 sec^{-1} at ~ 300 °K, which is consistent with the expected noncrossing of the $^30^+$ and $^30^-$ potentials shown in Fig. 1. At our Xe density of $\sim 10^{19}$ cm^{-3} this yields a transfer rate of $< 5 \times 10^4$ sec^{-1}, compared to the $6\,^3P_1$ decay rate of 10^7 sec^{-1} or $\sim 8 \times 10^6$ sec^{-1} with slight radiation trapping. Thus, at 300 °K less than 1% of the initially excited $6\,^3P_1$ atoms are transferred to $6\,^3P_0$ before radiative decay. This excitation transfer rate can increase with temperature, but is expected to remain negligible in our experiment. Those atoms

which are transferred to $6\,^3P_0$ can be expected to radiatively decay slowly by $^30^- - {}^10^+$ band emission in the $\lambda > 265$ nm region, or more likely to be quenched by molecular impurities. In either event, this $^30^- - {}^10^+$ band emission should be insignificant compared to the bands associated with the $6\,^3P_1 - 6\,^1S_0$ transition.

The interpretation of the data in Fig. 3 may be complicated by the possibility that it is due to overlapping $^30^+ - {}^10^+$ and $^31 - {}^10^+$ bands. There is apparently no significant quasistatic blue wing to the atomic resonance line, so both bands are expected to occur on the red wing. This indicates that the ^{31} level is more attractive than $^10^+$, which is reasonable. However, since ^{31} is expected to be much less attractive than $^30^+$, the $^31 - {}^10^+$ band should be confined to a much narrower wavelength range on the red wing. Also, due to the exponential population factors in Eq. (1) the $^31 - {}^10^+$ band should be weaker, with largest intensity relative to the $^30^+ - {}^10^+$ band at high temperatures. Kielkopf and Miller[11] have reported about 20 fairly regularly spaced (~ 15 cm^{-1}) emission peaks in the 254–265 nm region. These peaks may be due to bound–bound vibrational bands of the $^31 - {}^10^+$ transition, in which case this wavelength region represents the $^31 - {}^10^+$ band. (Another possible explanation is bound–bound bands of the $^30^+ - {}^10^+$ band from the R region of $^10^+$ state binding.) If the $^31 - {}^10^+$ band occurs predominantly in the 254–256 nm region, corre-
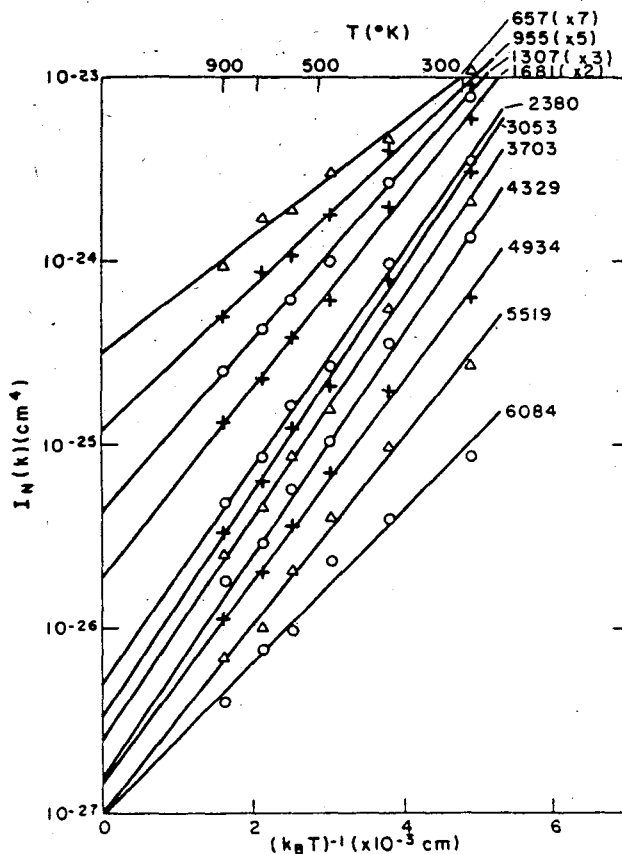

FIG. 4. The normalized HgXe 270 nm band intensity as a function of temperature, for selected wavelengths across the band. Values of $k_0 - k$ are given, as are multiplicative factors used for display convenience.
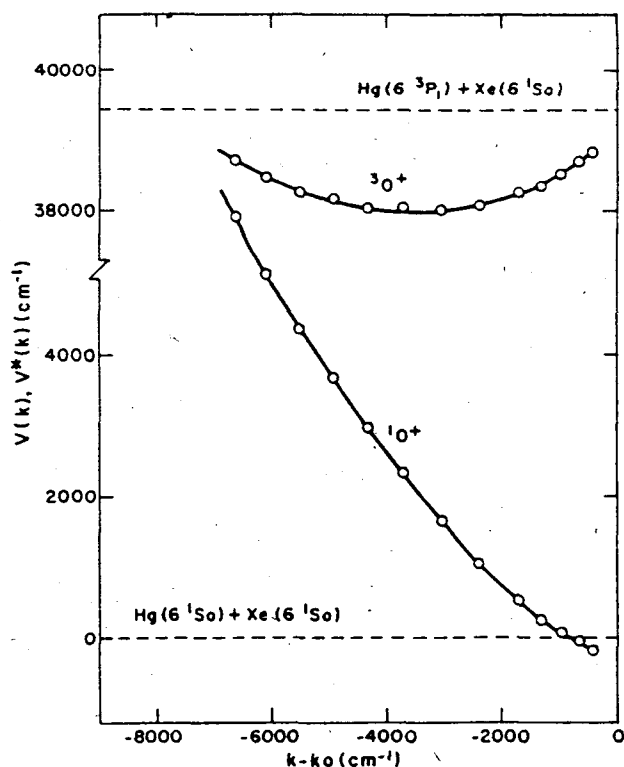
FIG. 5. HgXe excited and ground state potentials as a function of k.

sponding to $k_0 - k < 400$ cm^{-1}, then our data which extend from 256–300 nm should be entirely due to the $^3O^+ - ^1O^+$ band for $\lambda > 257$ nm; they would be slightly influenced by the $^31 - ^1O^+$ band at 256–257 nm although data given in the following paragraph indicate otherwise. In the following paragraph we will interpret the data on the assumption that they are due to the $^31 - ^1O^+$ band only. We will then return to the possible effect of an overlapping $^31 - ^1O^+$ band.

The absence of a satellite, or head of heads, at the red edge of the $^3O^+ - ^1O^+$ band, or anywhere else in the band, implies that $k(R)$ in Eqs. (1) and (2) is a monotonic function and $R(k)$ is single valued for the $^3O^+ - ^1O^+$ band. Each $\lambda \geq 256$ nm thus corresponds to a single $\Delta V^*(k)$ in Eq. (1), and the temperature dependence at k yields $\Delta V^*(k)$. A single-exponential fit is therefore expected at each k. In Fig. 4, $\log[I_N(k)]$ is plotted versus $1/k_B T$ for various λ. The points have been fitted by single exponentials (straight lines), and the intercepts at $T^{-1} = 0$ yield the $T = \infty$ curve in Fig. 3. It can be seen in Fig. 4 that a single-exponential fit is consistent with the data. The slopes of the fitted lines are the $\Delta V^*(k)$ given in Fig. 5, where $\Delta V(k) = \Delta V^*(k) + k_0 - k$ is also given, i.e., these are $V^*[R(k)] - V^*(\infty)$ and $V[R(k)] - V(\infty)$, where $V^*(R)$ is the $^3O^+$ and $V(R)$ the $^1O^+$ potentials. If equilibration of the bound states was insufficient at the lowest temperatures, as discussed in Sec. II, this would cause the apparent temperature dependence to be too gradual. A 30% increase in the lowest-temperature, band-peak intensity is as much as might be expected, and would cause about a 50 cm^{-1} increase in the $^3O^+$ well depth. Thus, the uncertainty in these

potentials is estimated as ± 100 cm^{-1}, due primarily to possibly systematic uncertainties in $I_N(k)$, so that we obtain -1400 ± 100 cm^{-1} for the $^3O^+$ state binding. The fact that $\Delta V^*(k)$ and $\Delta V(k)$ fit smoothly onto the other data at $k_0 - k = 430$ cm^{-1} implies that any intensity due to the $^31 - ^1O^+$ band is also relatively unimportant at this k. Furthermore, the $\log I_N(k)$ versus β plots (Fig. 4) appear linear over the entire temperature range, whereas curvature would result from the different exponential factors associated with two bands. This implies that the ^{31} state is not a significant radiator over the wavelength region studied (i.e., $k - k_0 > 500$ cm^{-1}). If, however, the $^31 - ^1O^+$ band radiation were present at a weak level not detected in the previous two checks, then the actual $^3O^+$ potential would be slightly more attractive than that shown in Figs. 5 and 6.

The R or k dependence of the $^3O^+ - ^1O^+$ transition moment $D(r)$ is not known, whereas it is required in Eq. (2) to obtain $V^*(R)$ and $V(R)$ from the data. It is nonetheless interesting to have an estimate of the R dependence of these potentials, so we will use indirect evidence to estimate $D(R)$. As noted in Sec. II, we expect the $^3O^+ - ^1O^+$ transition moment to decrease at small R, due to mixing of $^3P_{2,1,0}$ levels. If the transition moments were distributed equally between levels, this decrease would be a factor of 3. The R at which the $\Delta V(R)$ becomes comparable to the fine-structure splitting should be about the midpoint of this variation. This is approximately the behavior observed[6] in Hg$_2$. In the present case such a variation corresponds to decreasing $D(R)/D(\infty)$ by a factor of 1.5–2 in the neigh-
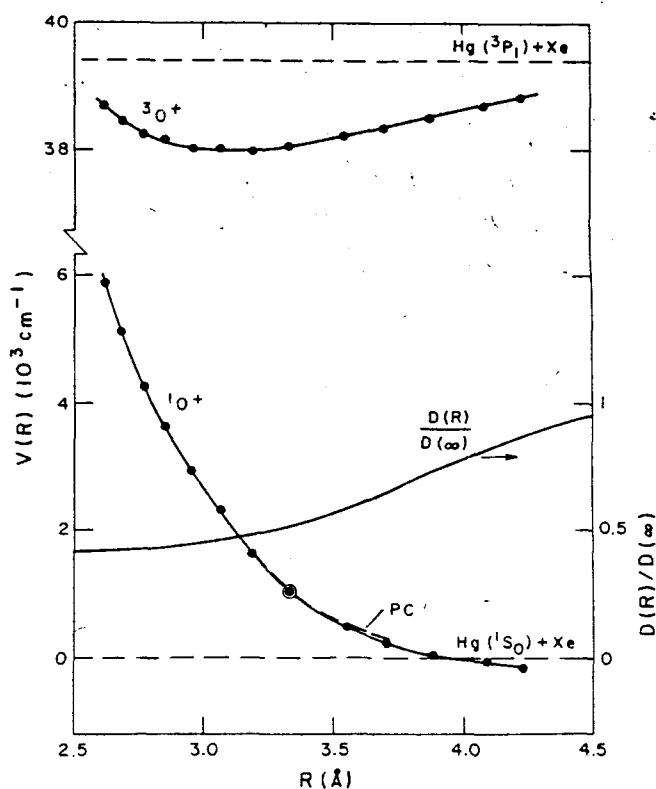

FIG. 6. HgXe excited and ground state potentials as a function of R. The dashed curve is from Powers and Cross (Ref. 12).

borhood of the $^3O^+$ state potential minimum. This amount of variation is strongly supported by the fact that the $^1O^+$ state $V(R)$ obtained from Eq. (2) then fits the $V(R)$ inferred from atomic beam scattering data.[12] For this comparison it is also necessary to choose the starting value R_1 in Eq. (2) to yield $V(R_1)$ in agreement with the scattering data. In essence, we match our $V(R)$ to the scattering $V(R)$ at one point $R_1 = 3.33$ Å in Fig. 6. The steepness of our $V(R)$ is then determined by the choice of $D(R)/D(\infty)$, and a value of ~ 0.6 yields good agreement with the $V(R)$ from scattering data. Thus, a decrease toward a factor of 2–3 reduction at small R is consistent with the Hg–Xe scattering data as well as with the Hg_2 $D(R)$ data and general theoretical expectations. In order to indicate the $V^*(R)$ and $V(R)$ which result from such assumptions we have taken

$$\frac{D(R)}{D(\infty)} = 1 - 0.6\, e^{-(R/4 \; Å)^8}$$

and $R_1(k = 37\,030\ \text{cm}^{-1}) = 3.33$ Å in Eq. (2). This $D(R)/D(\infty)$ and the resulting potentials are shown in Fig. 6, where $V(R)$ is compared to the scattering result.

VI. DISCUSSION

We have measured a $^3O^+$ well depth of $1400 \pm 100\ \text{cm}^{-1}$, which agrees very well with the estimate of $1300\ \text{cm}^{-1}$ inferred by Gutcheck et al.[2] from measurements in electron–beam excited vapors. Stransz et al.[13] gave a value of $1560\ \text{cm}^{-1}$ by fitting a Lennard-Jones type potential to low pressure, near-wing measurements, but as the near-wing results from only the long-range interaction and in addition is due to both the $^3O^+$ and ^{31} states, this agreement is accidental.

From Fig. 6 the van der Waals well depth in the ground $^1O^+$ state appears to be $\sim 200\ \text{cm}^{-1}$, but is not well determined in this experiment because the excimer bands were not reliably measured close to line center. As seen in Figs. 5 and 6, we have analyzed only that part of the excimer band that arises from the portion of the $^3O^+$ state bound by $>500\ \text{cm}^{-1}$. The $D(R)$ variation and R_1 value used in Eq. (2) to obtain the $^3O^+$ and $^1O^+$

potentials in Fig. 6 were chosen to yield a fit to the atomic–beam scattering $^1O^+$ potential. Nonetheless, this type of $D(R)$ variation is consistent with the theoretical expectations and measurements on Hg_2.

In conclusion, it appears that all observed spectra, excitation transfer rate coefficients, and scattering data are consistent with the adiabatic potentials in Figs. 1 and 6, whose general pattern is expected on theoretical grounds. However, the R dependence of these potentials are not accurately determined in this experimental analysis.

ACKNOWLEDGMENT

[1] J. R. Fuhr, W. L. Wiese, and L. J. Roszman, *Bibliography on Atomic Line Shapes and Shifts*, Natl. Bur. Stand. (U.S.) Spec. Publ. 366 (1972), Supplement 1 (1974) and Supplement 2 (1975).

[2] R. A. Gutcheck, R. M. Hill, D. L. Heustis, D. C. Lorents, and M. V. McCusker, "Studies of e-Beam Pumped Molecular Lasers," SRI Report #MP75-43 (August 1975).

[3] E. V. Nikiforov, L. I. Plimak, Yu. B. Predtechenskii, and L. D. Shcherba, Opt. Spectrosc. 41, 195 (1976).

[4] J. R. Woodworth, J. Chem. Phys. 66, 754 (1977).

[5] R. Scheps, Ch. Ottinger, G. York, and A. Gallagher, J. Chem. Phys. 63, 2581 (1975).

[6] E. W. Smith, R. E. Drullinger, M. M. Hessel, and J. Cooper, J. Chem. Phys. 66, 5667 (1977).

[7] G. Herzberg, *Spectra of Diatomic Molecules* (Van Nostrand, Princeton, 1950), 2nd edition, p. 224.

[8] R. E. M. Hedges, D. L. Drummond, and A. Gallagher, Phys. Rev. A 6, 1519 (1972).

[9] R. Scheps and A. Gallagher, J. Chem. Phys. 65, 859 (1976).

[10] J. S. Deech, J. Pitre, and L. Krause, Can. J. Phys. 49, 1976 (1971).

[11] J. F. Kielkopf and R. A. Miller, J. Chem. Phys. 61, 3304 (1974).

[12] J. R. Powers and R. J. Cross, J. Chem. Phys. 56, 3181 (1972).

[13] O. P. Stransz, J. M. Campbell, S. DePaoli, H. S. Sandhu, and H. E. Gunning, J. Am. Chem. Soc. 95, 732 (1973).